Flame Spray Pyrolysis of Electrode Materials for Energy Applications

Paul I. Dahl*, Magnus S. Thomassen, Luis C. Colmenares, Alejandro O. Barnett, Scott Lomas, Per E. Vullum, Sidsel M. Hanetho, Tommy Mokkelbost

SINTEF Materials and Chemistry, Trondheim, Norway
*Corresponding author: paul.inge.dahl@sintef.no, +47-98243955

ABSTRACT

Flame spray pyrolysis (FSP) was applied to produce nanopowders of $Ti_{1-x}M_xO_2$ and $Sn_{1-x}M_xO_2$, where x = 0.05 and M = Nb/Sb, for use as catalyst support materials in PEM fuel cells/ electrolysers. FSP powders in the SnO_2-IrO_2 system were produced for the same applications. Homogenous particle size distribution (5-20 nm) was demonstrated by TEM, supported by BET and XRD analysis. Whereas two polymorphs were indicated for the Ti-based oxides, the Sb/Nb-doped SnO_2 powders were single phase. FSP powders of Mn_3O_4 intended for supercapacitors were produced and the influence of the precursor/solvent mixtures on the physical and electrochemical properties evaluated.

INTRODUCTION

Nanostructured materials are gaining widespread use, which requires new approaches to powder synthesis, in particular with respect to increased production while maintaining proper safety procedures. Flame spray pyrolysis (FSP) is an excellent tool for pioneering development of complex nanomaterials for various applications and at the same time being a scalable process already being investigated by commercial powder producers [1]. Such nanomaterials are of interest for electrodes in various energy applications e.g. PEM fuel cells and electrolysers or supercapacitors. For these applications there are strong material requirements, and nanopowders with high conductivity, high surface area, well defined and sustainable pore structure/size distribution, stability and corrosion resistance are needed [2, 3].

In the present work FSP is applied to produce and investigate properties of titanium- and tin-based oxide powders for use as cathode catalyst support materials for PEM fuel cells and PEM electrolysers. TiO_2 materials are of interest due to high stability and corrosion resistance, however, doped SnO_2 is more widely studied for this application [4-6]. TiO_2- and SnO_2-based materials are already reported synthesized by FSP in the literature, and typical precursors for Ti and Sn are titanium isopropoxide [1, 7] and tin 2-ethylhexanoate [8, 9], respectively.

For supercapacitors, manganese oxides are promising alternatives to carbon electrodes as they offer high specific capacitance, low cost, abundance and have an environmentally friendly nature [8, 10]. Whereas Mn_2O_3 is reported produced by FSP in the literature [11, 12], MnO_2 or Mn_3O_4 are to the authors' knowledge not reported elsewhere. It is hence of interest to tailor the FSP conditions and precursor solutions to obtain the various phases of Mn-oxides. Reported Mn-precursors applied for FSP are manganese nitrate [11, 12], manganese acetate [13, 14], manganese acetylacetonate and manganese 2-ethylhexanoate [15]. In the present work the effect of Mn-precursor and solvent system will be investigated, with respect to microstructure, crystallite-/ particle size, porosity and electrochemical properties of Mn_3O_4 powders produced by FSP.

EXPERIMENTAL

Nanostructured powders based on TiO_2 and SnO_2 doped with Nb or Sb, powders in the SnO_2-IrO_2 system, as well as Mn_3O_4 were produced by flame spray pyrolysis (NPS10, Tethis S.p.A.). The composition of prepared powders along with the precursors and solvents are listed in Table I. Additionally sucrose was used as an additive for one of the Mn_3O_4 precursor solutions. The precursor/solvent mixtures were sprayed into a flame (CH_4/O_2 flow rates: 1.5/3.0 L/min) using a liquid flow rate of 5 mL/min and 5 L/min flow of dispersion gas (oxygen or nitrogen). A pressure drop (dispersion gas at nozzle tip) of ~2.0 bars was used and the powders were collected on a glass microfiber filter (Whatman GF6).

Table I. Composition, precursors and solvents used for the production of FSP powders.

Composition	Precursors	Solvent
TiO_2	Titanium(IV) isopropoxide	p-Xylene
$Ti_{0.95}Nb_{0.05}O_2$	Titanium(IV) isopropoxide Niobium(V) ethoxide	p-Xylene
SnO_2	Tin(II) 2-ethylhexanoate	p-Xylene
$Sn_{0.95}Nb_{0.05}O_2$	Tin(II) 2-ethylhexanoate Niobium(V) ethoxide	p-Xylene
$Sn_{0.95}Sb_{0.05}O_2$	Tin(II) 2-ethylhexanoate Antimony(III) ethoxide	p-Xylene
SnO_2-IrO_2	Tin(II) 2-ethylhexanoate Iridium(III) acetylacetonate	Toluene
Mn_3O_4	Manganese(II) acetate tetrahydrate Mn(III) acetylacetonate	Water or 50% ethanol Acetyl acetone

The as-synthesized powders were dispersed in ethanol and a droplet was transferred to a holey carbon coated Cu TEM-grid. TEM was performed with a double Cs corrected, coldFEG JEM ARM200F, operated at 200 kV. Further analysis of specific surface area and pore size distribution was performed through N_2 adsorption/desorption measurements (Micromeritics Tristar). The powders were studied by X-ray diffraction (XRD) using a Bruker D8 Focus diffractometer with Cu Kα radiation and LynxEye detector. The diffraction data was analyzed using the Rietveld method as implemented in the TOPAS software by Bruker. Thermo gravimetric analysis (TGA) (Netzsch STA 449C *Jupiter*) was performed on as-synthesized Mn_3O_4 powders in synthetic air with a heating rate of 10 °C/min to 1000 °C.

Two-probe measurements were performed on compressed (~56 bar) oxide powders to determine the electronic conductivities. Based on the measured height of the powder column between two pistons, the apparent conductivities of the samples were determined by applying (at a scan rate of 20mV/s) the following bias sequence: *1)* 100 cycles between -200 and 200 mV, *2)* 70 cycles between -400 and 400 mV, *3)* 100 cycles between -200 and 400 mV. The apparent conductivity is reported as an average of the number of applied cycles.

The electrochemical response of MnO_3O_4 was tested in a three electrode configuration. The working electrodes (WE) were prepared from slurry (sonicated mix of MnO_3O_4 powder, Nafion, isopropanol, water) and applied to an Au-disk electrode. These electrodes contained 0.163-0.167 mg MnO_3O_4 with 10 wt% Nafion after drying. Pt wire was used as the counter electrode (CE)

and a standard reference electrode (RHE) was used while 0.5 M Na_2SO_4 saturated with N_2 was used as electrolyte. The electrodes were cycled 50 times between 0.1 and 0.9 V vs. RHE at a sweep rate of 50 mV·s^{-1} in order to obtain stable and reproducible voltammograms.

RESULTS

The morphology in nanostructured FSP powders of TiO_2, $Ti_{0.95}Nb_{0.05}O_2$ and $Sn_{0.95}Nb_{0.05}O_2$ is depicted in Figure 1. In general the crystallites have a quite narrow size distribution (5-20 nm), however, some larger particles (~100 nm) are observed in the $Ti_{0.95}Nb_{0.05}O_2$ powder.
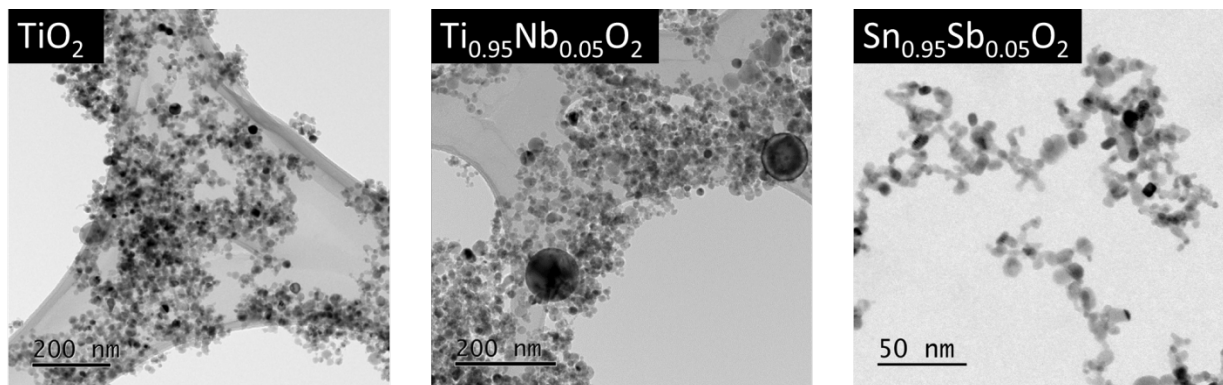
Figure 1. TEM micrographs indicating morphology and crystallite-/particle size

The phase compositions and crystallite size from XRD/Rietveld refinements and BET surface area/particle size of the Ti-based powders are presented in Table II, while lattice parameters, crystallite size and surface area/particle size of the Sn-based powders are presented in Table III.

Table II. Crystal structures/crystallite size from X-ray diffraction/Rietveld method and surface area and estimated particle size from nitrogen adsorption (BET) for TiO_2-based materials.

Composition		TiO_2	$Ti_{0.95}Nb_{0.05}O_2$
Phase composition	Anatase (wt%)	77.6	77.3
	Rutile (wt%)	22.7	-
	β-TiO_2 (wt%)	-	22.7
XRD crystallite size (nm)		A: 16.3 / R: 6.2	A: 16.8 / β: 8.8
BET surface area (m²/g) / particle size (nm)		109 / 13	104 / 14

Table III. Lattice parameters/crystallite size from X-ray diffraction/Rietveld method and surface area and estimated from nitrogen adsorption (BET) for SnO_2-based materials.

Composition		SnO_2	$Sn_{0.95}Nb_{0.05}O_2$	$Sn_{0.95}Sb_{0.05}O_2$
Lattice parameters (P42/mnm)	a (Å)	4.738	4.739	4.739
	c (Å)	3.189	3.189	3.187
XRD crystallite size (nm)		9.5	9.1	8.7
BET surface area (m²/g) / particle size (nm)		91.5 / 9.4	102 / 8.4	102 / 8.4

Both the average crystallite size derived from Rietveld refinement and the measured surface areas are in line with the TEM micrographs, and the crystallites appear to be slightly smaller in

the Sn-based powders. Anatase is the dominating phase in both powders and the secondary phase of Rutile, present in TiO_2 is replaced by β-TiO_2 when doping with Nb.

The SnO_2, $Sn_{0.95}Nb_{0.05}O_2$ and $Sn_{0.95}Sb_{0.05}O_2$ all appeared single phase by XRD. Evaluation of the valance in the Nb-/ Sb-doped powders based on the slight change in lattice parameters for the as compared to the SnO_2 samples is uncertain as the powders are nanocrystalline. XRD results on the SnO_2-IrO_2 powders indicate a two-phase system with some solid solution of Ir in SnO_2 and Sn in IrO_2. More crystalline powders are required to quantify the solid solubility.

The pore size distribution in these materials is comparable to those obtained for the other SnO_2-based powders and commercial carbon reference material used for catalyst support, as demonstrated in Figure 2.
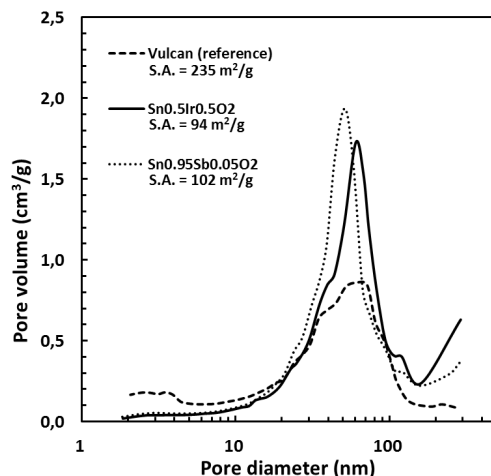

Figure 2. Pore size distribution and surface area in SnO_2-based powders v Vulcan reference.

The conductivity of the SnO_2-IrO_2 samples was found to increase from 0.013 S/cm to 0.155 S/cm when the Ir:Sn molar ratio was increased from 3:7 to 1:1. In comparison a reference powder of SnO_2 with 20wt% Ir catalyst deposited showed a conductivity of 0.117 S/cm. There is room for further optimization of the molar ratio Ir:Sn. It is reported that the specific activity is constant up to a ratio of 1:1, beyond which it decreases [16].

The effect of the precursor/solvent system is demonstrated for FSP powders of Mn_3O_4, as seen for morphology and crystallite-/particle size in Figure 3, and TGA/XRD in Figure 4. While a complete combustion and rapid crystallization produces homogenous nanopowders when acetyl acetone is used, 50 % ethanol gives a more crystalline, but less homogenous powder. Addition of sucrose results in a slower and incomplete combustion with significant organic residue.

Figure 5 a) shows the effect of the precursor/solvent system applied and the pore size distribution and surface area of Mn_3O_4. The pore size distribution seems to narrow down as the solvent becomes more flammable, i.e. when going from water to 50 % ethanol to acetyl acetone. The addition of sucrose appears to eliminate most of the porosity seen in the other samples, possibly due to pore blocking from residual organics.

Figure 5 b) shows voltammograms with currents normalized with respect to mass of Mn_3O_4. All three materials show a reduction peak between 0.33 and 0.36 V vs. RHE and a considerable decrease in specific current at lower potentials. In the anodic direction, a large increase in current is observed. However, the onset potential for the oxidation is different for the three types of materials. In general, the materials show similar electrochemical behaviour, but considerable differences in the magnitude of the specific currents.
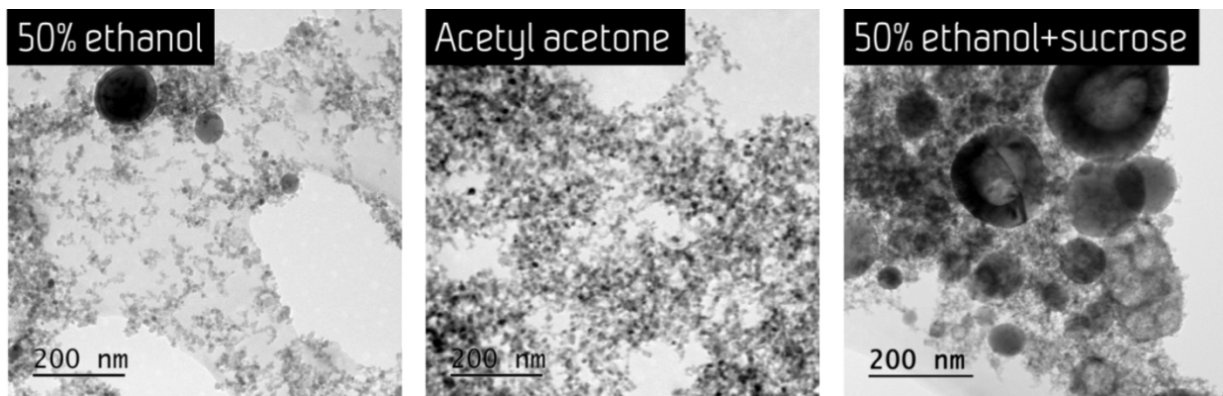
Figure 3. TEM micrographs indicating the effect of precursor solutions on powder morphology and crystallite- / particle size in Mn_3O_4 powders.

a)
b)
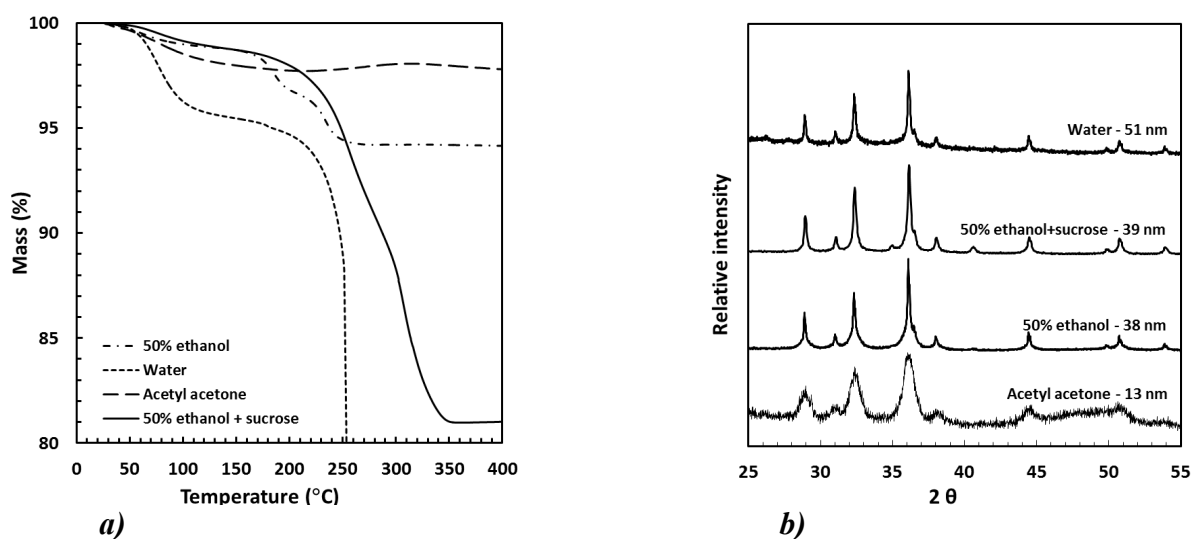
Figure 4. a) TGA and b) XRD indicating degree of combustion and crystallization of the Mn_3O_4 powders synthesized with different procedures.

a)
b)
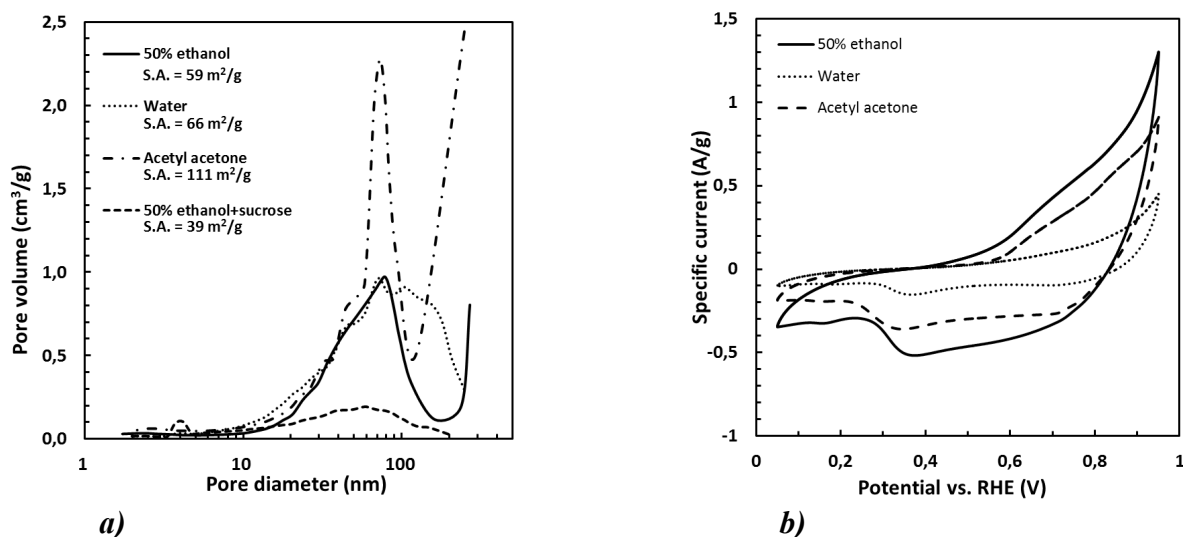
Figure 5. a) Pore size distribution/surface area, and b) Voltammograms of Mn_3O_4 materials.

CONCLUSION

Nanopowders of promising oxide materials for use in electrodes for energy applications were prepared by flame spray pyrolysis. Results from TEM, BET and XRD agree on crystallite-/ particle sizes in the range of 5-20 nm in samples prepared with highly combustible precursor solutions. These powders showed high surface area, i.e. ~100 m^2/g and a pore size distribution comparable to that of commercially available carbon electrode materials. The effect of different precursor solutions on combustion, crystallization, morphology, size distributions and electrochemical properties was demonstrated using water, 50 % ethanol and acetyl acetone as solvents. Addition of carbon source in the precursor solution, aiming for oxide-carbon composite materials results in an organic residue, however, this also appears to clog the porous structure.

REFERENCES

1. Teoh, W.Y., Amal, R., Madler, L., Nanoscale, 2010. **2**(8): p. 1324-1347.
2. Sharma, S., Pollet, B.G., Journal of Power Sources, 2012. **208**: p. 96-119.
3. Rabis, A., Rodriguez, P., Schmidt, T.J., Acs Catalysis, 2012. **2**(5): p. 864-890.
4. Takasaki, F., Matsuie, S., Takabatake, Y., Noda, Z., Hayashi, A., Shiratori, Y., Ito, K., Sasaki, K., Journal of the Electrochemical Society, 2011. **158**(10): p. B1270-B1275.
5. Tsukatsune, T., Takabatake, Y., Noda, Z., Hayashi, A., Sasaki, K., Polymer Electrolyte Fuel Cells 10, Pts 1 and 2, 2013. **58**(1): p. 1251-1257.
6. Kanda, K., Noda, Z., Nagamatsu, Y., Higashi, T., Taniguchi, S., Lyth, S. M., Hayashi, A., Sasaki, K., ECS Electrochemistry Letters, 2014. **3**(4): p. F15-F18.
7. Teleki, A., Bjelobrk, N., Pratsinis, S.E., Sensors and Actuators B: Chemical, 2008. **130**(1): p. 449-457.
8. Grossmann, K., Kovacs, K. E., Pham, D. K., Madler, L., Barsan, N., Weimar, U., Sensors and Actuators B-Chemical, 2011. **158**(1): p. 388-392.
9. Madler, L., Roessler, A., Pratsinis, S. E., Sahm, T., Gurlo, A., Barsan, N., Weimar, U., Sensors and Actuators B-Chemical, 2006. **114**(1): p. 283-295.
10. Zhang, S.W., Chen, G.Z., Energy Materials: Materials Science and Engineering for Energy Systems, 2008. **3**(3): p. 186-200.
11. Karthikeyan, J., Berndt, C. C., Tikkanen, J., Wang, J. Y., King, A. H., Herman, H., Nanostructured Materials, 1997. **8**(1): p. 61-74.
12. Tikkanen, J., Gross, K. A., Berndt, C. C., Pitkanen, V., Keskinen, J., Raghu, S., Rajala, M., Karthikeyan, J., Surface & Coatings Technology, 1997. **90**(3): p. 210-216.
13. Liu, G., Yue, R. L., Jia, Y., Ni, Y., Yang, J., Liu, H. D., Wang, Z., Wu, X. F., Chen, Y. F., Particuology, 2013. **11**(4): p. 454-459.
14. Kim, J.H., Choi, S. H., Son, M. Y., Kim, M. H., Lee, J. K., Kang, Y. C., Ceramics International, 2013. **39**(1): p. 331-336.
15. Ernst, F.O., Kammler, H. K., Roessler, A., Pratsinis, S. E., Stark, W. J., Ufheil, J., Novak, P., Materials Chemistry and Physics, 2007. **101**(2-3): p. 372-378.
16. Marshall, A., Børresen, B. Hagen, G., Tsypkin, M., Tunold, R., Electrochimica Acta, 2006. **51**(15): p. 3161-3167.